

A Scalable High-Gain and Large-Beamwidth mm-wave Harvesting Approach for 5G-powered IoT

Aline Eid, Jimmy Hester, and Manos M. Tentzeris

School of Electrical and Computer Engineering, Georgia Institute of Technology, Atlanta, GA, USA.

Abstract—In this effort, the authors demonstrate for the first time the implementation of a Rotman-Lens-based rectenna system for mm-wave harvesting, in the 28 GHz band. The structure merges unique RF and DC combination techniques, for the realization of rectennas that display the unlike combination of high gain and large beamwidth. The Rotman-lens-based rectenna includes components—antennas, rectifiers, Rotman lens, and power combining network—whose design is first presented and performance is experimentally characterized and verified. Then, the fabrication and testing of the device, and that of a reference design—comprising a DC-combined array of rectennas of equal aperture—is presented. The novel Rotman-based rectenna harvester shows a 21-fold increase in the harvested power compared to its reference counterpart, while its angular coverage remains identical. The structure, therefore, demonstrates the surprising combination of high-gain and large beamwidth, thereby potentially enabling the emergence of passive long-range mm-wave RFIDs.

Keywords—5G, energy harvesting, wireless power transfer, IoT, millimeter-waves, rectenna, rectifying circuit, flexible printed electronics.

I. INTRODUCTION

The current era is witnessing a rapid development in the field of mm-wave and IoT technologies with a projected 50 billion IoT devices to be installed by 2020. This would imply that a huge number of batteries need be continuously charged and replaced. The design and realization of energy-autonomous, self-powered systems is therefore highly desirable. One potential way of satisfying these goals is through electromagnetic energy harvesting. A powerful source for electromagnetic scavenging is mm-wave energy, taking place in the 5G bands (above 24 GHz), where the limits of allowable transmitted power by the FCC regulations are pushed beyond that of their lower-frequency counterparts. In addition to the advantage of high transmitted power available at 5G, moving to mm-wave bands allows the realization of modular antennas array instead of a single elements, thereby allowing a fine scaling of their antenna aperture. However, one limitation accompanies large gain antennas: their inability to provide an isotropic radiation. As the relative orientations of the sources and harvesters are generally unknown, the use of large aperture mm-wave harvesters may seem limiting and impossible. Individual rectennas, constituted of small antenna elements, can realistically be DC combined. However, this approach does not increase the sensitivity (lowest turn-on power) of the overall rectenna system: RF combination is needed. Beamforming networks (BFNs) are used to effectively create simultaneous beam coverage with large-gain arrays, by mapping a set of directions to a set of feeding ports. The Rotman lens, introduced in the 1960s, constitutes one the

most common designs for BFNs and is commonly utilized to enable multibeam phased array system [1] and wide-band operation, thanks to its implementation of true-time-delays. In this paper, and for the first time, the capabilities of a BFN (in the form of a Rotman lens) are implemented to enable the surprising combination of high gain and large beamwidth energy harvesting through quasi-isotropic RF combining. Because the lens is capable of focusing the energy coming from a given direction into its geometrically-associated beam port, the proposed scheme loads each of these ports with a rectifier, thereby channeling the energy coming from any direction to one of the rectifiers. The DC outputs of the rectifiers are then serially combined to feed the rectified power to the load, regardless of which one is providing the power.

II. 28 GHz HARVESTER BASIC ELEMENTS

A. Series-Fed Antenna Array Design

The realization of antenna arrays at mm-wave frequencies is desirable and potentially scalable, thereby enabling a fine control over the aperture of the antenna. Also, antennas can be arrayed over the vertical axis, while still largely covering the 2D landscape of most environments. Due to its simplicity, broad beamwidth, and metal backing, patch antennas were used for this work and arranged in series-fed antenna arrays. The antenna, whose schematic is presented in Fig. 1a, was printed on copper-clad Liquid crystal polymer (LCP) substrate ($\epsilon_r = 3.02$ and $h = 180 \mu\text{m}$) using an inkjet-printed masking technique followed by etching. This antenna array consists of five serially-fed patch antennas with dimensions shown in Fig. 1a, providing an operation centered at 28.55 GHz with a reflection coefficient S_{11} lower than -20 dB within this range. Their vertical beamwidth of about 20° (provided by the five antennas) is appropriate for most use cases, where environments expand mostly horizontally. Its simulations showed a gain of 13 dBi and a beamwidth of 80° in the plane perpendicular to the linear array.

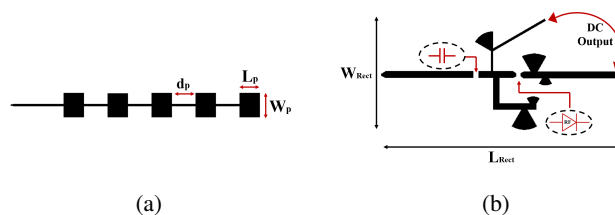


Fig. 1. (a) Schematic of the series-fed patch antenna array with $W_p = 3.35\text{mm}$, $L_p = 2.9\text{mm}$ and $d_p = 3.32\text{mm}$, (b) Layout of the designed 28GHz rectifier with $L_{rect} = 19\text{mm}$ and $W_{rect} = 9\text{mm}$

B. 28 GHz Rectifier Design

Mm-wave energy harvesting requires the use of a diode with low series resistance and high cut-off frequency. Therefore, the designed rectifier consists of a packaged gallium arsenide beam-lead Schottky barrier diode from Macom (MA4E2038 model). A rectifier, shown in Fig. 1b, was designed, assembled, and tested. Its via-less layout consists of a $50\ \Omega$ feed line followed by an ultra-broadband capacitor (with an operation up to 40 GHz) used as a dc block, the reason for which will be explained later in this paper. The dc block is followed by a quarter-wave radial stub in the upper side of the design, providing a virtual short-circuit used to isolate a DC port on this side of the rectifying diode. An L-network is then used to provide proper matching at the input of the diode, while two quarter-wave radial stubs finally added as a virtual short-circuit for the fundamental and second harmonic byproducts of the rectification. The structure was then simulated, using same proven model reported in [2]. The rectifier was printed on a $180\ \mu\text{m}$ thick copper-clad Rogers LCP substrate, using the aforementioned inkjet printing and etching technique, and measured to produce the results shown in Fig. 2. Both simulated and measured voltages and power-conversion efficiencies (PCEs), for an input power ranging between $-10\ \text{dBm}$ and $20\ \text{dBm}$ with the optimal $1\ \text{k}\Omega$ load of the structure, demonstrated better than $-7\ \text{dB}$ matching at $28.5\ \text{GHz}$ over the entire power sweep. The rectifier demonstrates a very high sensitivity relative to the literature [2], with a turn-on power of as low as $-10\ \text{dBm}$. In addition, a constant increase in the output voltage and efficiency until $20\ \text{dBm}$ is observed. This expected increase in efficiency as a function of RF input power provides the motivation for the architecture described in this paper. In other words: RF combining, if conducted with minimal losses, should outperform DC combining.

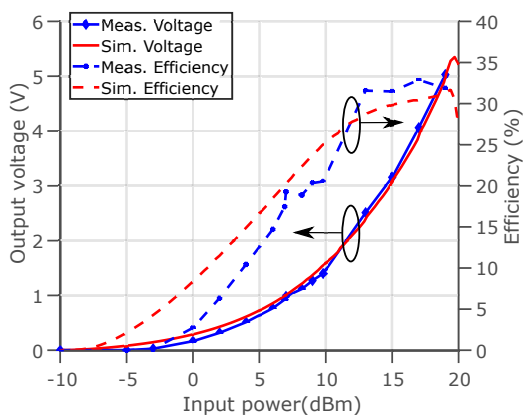


Fig. 2. Plot of the simulated and measured voltages and power conversion efficiencies of the designed 28 GHz rectifier.

III. ROTMAN LENS DESIGN

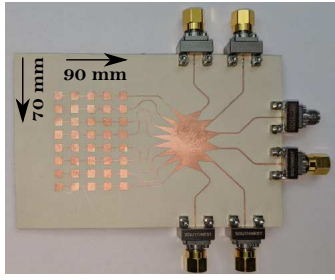
The Rotman lens operates just like an optical lens, by introducing differential propagation time delays to wavefronts

impinging onto the various points on its surface. By properly tuning the shape of the lens according to the geometrical optics approximation with the goal of focalizing plane waves impinging on the antenna side of the lens to different focal points on the beam-ports side of the lens, one achieves a lens-shaped structure with two angles of curvatures: one on the beam-ports side, and the other on the antenna side. When this process is applied properly, the structure maps a set of selected radiation directions to an associated set of beam-ports (ideally, one direction per port). Tappers are then added on both sides of the lens to create smooth impedance transitions from the input impedance of the antenna, to that experienced by the wave in the lens and, consequently, from the lens to the impedance of the beam ports. Such a structure, including eight antenna ports and six beam ports—and, therefore, six radiating directions—was designed, simulated, and tuned. Eight of the linear antenna arrays introduced in Sec. II-A were then added to the antenna ports of the array, and its beam-ports were extended by microstrip lines to enable their connection to end-launch $2.9\ \text{mm}$ connectors. In this configuration, six beams were chosen to intersect at angles providing $3\ \text{dB}$ lower gain than broadsight. Eight antennas provide a $3\ \text{dB}$ -beamwidth of 15° , which covers a total of $6 \times 15^\circ = 90^\circ$ in front of the array. The design was then also printed on flexible LCP substrate, resulting in the structure shown in Fig. 3a. It is important to note that the lens was designed with the assumption that a wave impinging in a direction normal to the plane of the antenna would arrive with the same time delay at all antenna ports of the lens. In order for this condition to be respected, meanders (characteristic of Rotman-lens-based arrays) were added to the connections between the antennas and the lens.

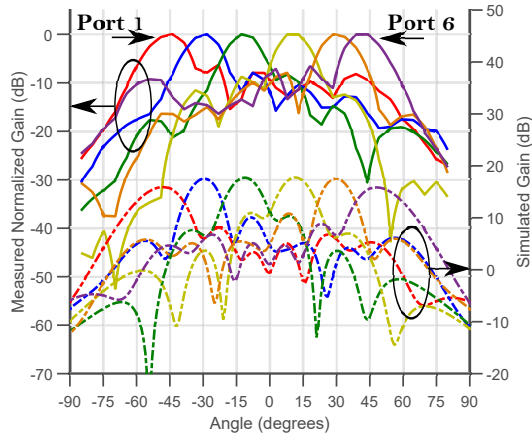
The radiation properties of the lens-based antenna system were simulated using the time-domain solver of CST STUDIO SUITE 2018, resulting in the six gain and radiation patterns shown in Fig. 3b. Precise measured gain patterns remained elusive due to the complexity of the de-embedding of the losses introduced by the additional microstrip line lengths that were necessary to provide enough space for the interfacing $2.9\ \text{mm}$ connectors. The ports were measured two-by-two with the unused ports terminated by $50\ \Omega$ loads, to guarantee the proper operation of the lens. Both simulated and measured radiation patterns (shown in shown in Fig. 3b) display a remarkable similarity, thereby validating the operation of the antenna array.

IV. ROTMAN LENS-BASED RECTENNA

In the previous section, it was demonstrated that the aggregated response of the all the channels of the Rotman can cover a large angular space. The use of the Rotman lens as an intermediate component between the receiving antennas and the rectifiers could, therefore, help maintain a stable output regardless of the sources location if the rectified products of each of the ports were combined. This achievement is extremely critical in practical conditions where the location of the RF source is unknown, making it necessary to achieve high gain and wide coverage simultaneously. In this section,



(a)



(b)

Fig. 3. (a) Picture of the flexible Rotman-lens-based antenna array and (b) Measured and simulated radiation patterns and gains, respectively, of the antenna array

the rectifier design shown in Sec. II and the Rotman-lens-based array presented in Sec. III were combined for this effect. This architecture consists of a series of eight parallel antennas attached to the Rotman lens from one side facing six rectifiers at the opposite side where DC serial combination is implemented. The structure essentially encompasses a first RF combining step, enabled by the lens, followed with a DC combining step, using the specifically-designed combining circuit presented in Fig. 4.

A. DC combining network

Power summation is very critical when it comes to unbalanced rectification outputs produced from realistic RF sources, and can be implemented differently depending on its costs and benefits [3]. This paper does not rely on a direct voltage summation topology (i.e. back-to-back RF diodes); however, it introduces a minimalist architecture relying on a total of $2 \cdot N$ bypass diodes, where N is the number of RF or rectifying diodes. Equipped with a low turn-on voltage of 0.1 V, the Toshiba 1SS384TE85LF bypass diodes used in the presented scheme creates a current path around all other rectifiers. This topology is optimal when only one diode is turned on, which can be assumed if a single, dominant source of power irradiates this particular design from a given direction. As described in [3], an equivalently optimal serial-combining network with independent but connected rectennas

requires $0.5 \times (N - 1)(N + 2)$ low-bias diodes, which can quickly become untenable upon scaling. The combining circuit therefore scales with one lesser order in number of diodes with the Rotman approach than it does with DC combination alone.

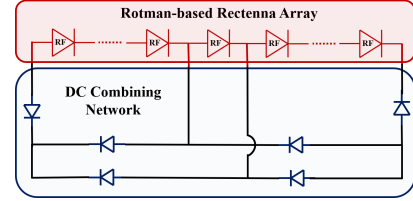


Fig. 4. Rotman-based rectenna power summation network.

B. Performance of the system

This combination resulted in the Rotman-based rectenna shown in Fig. 5, comprising both RF and DC combination networks: respectively, the Rotman lens and the DC-combining circuit. It is now obvious why the DC block capacitors were essential in this configuration. Without them, all six rectifiers would be connected to the Rotman lens. In addition to the aforementioned rectenna, a reference structure excluding the Rotman lens, comprising eight parallel rectennas (and, therefore, eight diodes), was designed and printed as shown in Fig. 5. It should be noted that the optimal DC combination network would have necessitated 35 diodes. It was, therefore, chosen to terminate this non-Rotman-based rectenna array with a direct serial combining network: since all the rectifiers in this structure are expected to be excited at the same time in the controlled testing environment, this simple DC combining scheme should provide good (although not optimal [3]) performance.

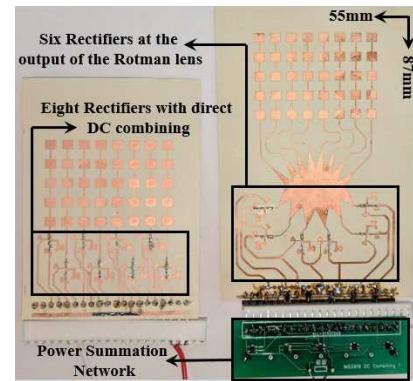


Fig. 5. Picture of the simple rectenna design (left) and the Rotman-based rectenna (right).

The two rectennas (Rotman and non-Rotman-based) were first characterized as a function of their received power density. Both were angularly positioned at their optimal harvesting angle and illuminated with a horn antenna with a gain of 20 dBi, placed at a distance of 52 cm away from the rectenna array, and outputting powers ranging from 18 dBm to 31 dBm. The two arrays were loaded with their optimal load

impedances of $1\text{ k}\Omega$ and $8\text{ k}\Omega$ respectively, and their produced voltage measured. The results of this experiment are shown in Fig. 6, where the harvested voltages and powers of both arrays are shown. It can be observed that, at low powers (where small increments in the RF power level translate to large differences in the efficiency of the rectifiers), the differences between both arrays is very pronounced; with incident power densities of less than -2 dBm cm^{-2} , the DC-combined rectenna does not even output any power, while its Rotman-based counterpart effortlessly produces an output. The Rotman-based rectenna turns on well below -6 dBm cm^{-2} , which compares quite favorably to the literature [4].

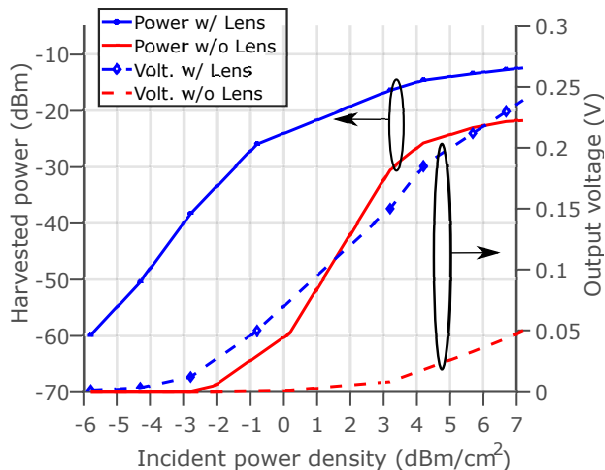


Fig. 6. Plot of the measured voltages and output powers versus incident power density for the rectenna with and without the Rotman Lens.

Both arrays were, as well, characterized for their responses over different angles of incidence. For this experiment, both arrays were tested near the turn-on power density of the simple rectenna array: 0 dBm cm^{-2} . This was achieved by placing the arrays 77 cm away from the same setup described in the previous paragraph (shown in Fig. 7), while these were precisely rotated in angular increments of 5° . Over an angular range of more than 90° in front of it, the Rotman-based rectenna conserves a high harvested power. This power oscillates between maxima observed in the directions of the main lobes of the Rotman network, and minima in between them. In this range, the Rotman-based architecture significantly outperforms its simple counterpart in all but two angular directions. The increase in harvested power enabled by the architecture is also plotted in Fig. 8, demonstrating the functional difference between the two arrays. The average of the Rotman-based array's harvested power (in natural scale) over all angles shows a 21-fold gain relative to that of its simple counterpart. In practical terms, this means that, in a context with randomly-positioned sources in space, this Rotman-based architecture would harvest 21 times the power of the non-Rotman based harvester, while preserving its angular coverage. It, therefore, achieves a remarkable and surprising combination of high gain and large angular coverage.

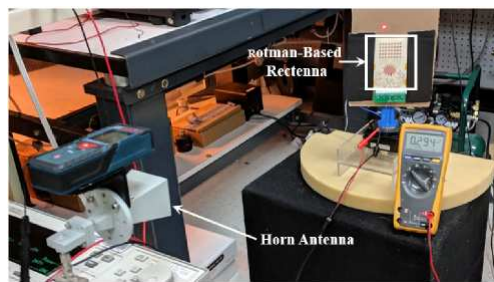


Fig. 7. Picture of the setup used to measure the angular response of the rectennas.

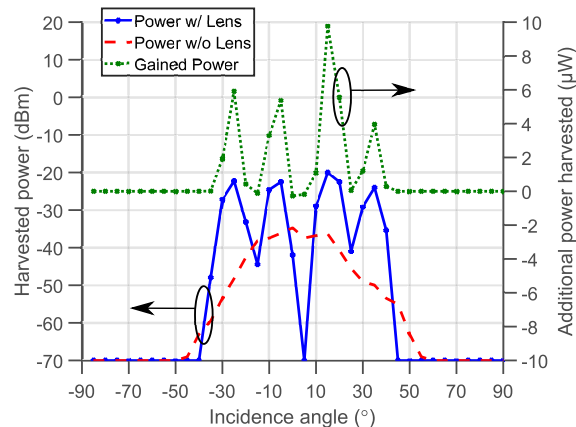


Fig. 8. Plot of the measured harvested power versus angle of incidence for the rectenna with and without the Rotman Lens.

V. CONCLUSION

This paper demonstrated an effective and, more importantly, very scalable method for the design of arbitrarily-sized and highly-sensitive mm-wave harvesters, without sacrificing their angular coverage. With the advent of 5G networks and their associated high allowed EIRPs, such properties may trigger the emergence of 5G-powered nodes for the IoT and ,combined with the long-range capabilities of mm-wave ultra-low-power backscatterers [5], of long-range passive mm-wave RFIDs.

REFERENCES

- [1] K. Wang, J.-F. Gu, F. Ren, and K. Wu, "A multitarget active backscattering 2-d positioning system with superresolution time series post-processing technique," *IEEE Transactions on Microwave Theory and Techniques*, vol. 65, no. 5, pp. 1751–1766, 2017.
- [2] J. Bito, V. Palazzi, J. Hester, R. Bahr, F. Alimenti, P. Mezzanotte, L. Roselli, and M. M. Tentzeris, "Millimeter-wave ink-jet printed rf energy harvester for next generation flexible electronics," in *Wireless Power Transfer Conference (WPTC), 2017 IEEE*. IEEE, 2017, pp. 1–4.
- [3] A. N. Parks and J. R. Smith, "Active power summation for efficient multiband rf energy harvesting," in *Microwave Symposium (IMS), 2015 IEEE MTT-S International*. IEEE, 2015, pp. 1–4.
- [4] S. Ladan, A. B. Guntupalli, and K. Wu, "A high-efficiency 24 ghz rectenna development towards millimeter-wave energy harvesting and wireless power transmission," *IEEE Transactions on Circuits and Systems I: Regular Papers*, vol. 61, no. 12, pp. 3358–3366, 2014.
- [5] J. G. Hester and M. M. Tentzeris, "A mm-wave ultra-long-range energy-autonomous printed rfid-enabled van-atta wireless sensor: At the crossroads of 5g and iot," in *Microwave Symposium (IMS), 2017 IEEE MTT-S International*. IEEE, 2017, pp. 1557–1560.